Numerical Consistency of Metric Terms in Terrain-Following Coordinates

JOSEPH B. KLEMP AND WILLIAM C. SKAMAROCK

National Center for Atmospheric Research, Boulder, Colorado*

OLIVER FUHRER

Atmospheric and Climate Science, ETH, Zurich, Switzerland

(Manuscript received 12 April 2002, in final form 14 November 2002)

ABSTRACT

In numerically integrating the equations of motion in terrain-following coordinates, care must be taken in treating the metric terms that arise due to the sloping coordinate surfaces. In particular, metric terms that appear in the advection and pressure-gradient operators should be represented in a manner such that they exactly cancel when transformed back to Cartesian coordinates. Noncancellation of these terms can lead to spurious forcing at small scales on the numerical grid. This effect is demonstrated for a mountain wave flow problem through analytic solutions to the linear finite-difference equations. Further confirmation is provided through numerical simulations with a two-dimensional prototype version of the Weather Research and Forecasting (WRF) model, and with the Canadian Mesoscale Compressible Community (MC2) model.

1. Introduction

Terrain-following coordinates have a long history of use in atmospheric simulation models, being first introduced in pressure coordinate models by Phillips (1957). Over the years, researchers have recognized that increased truncation errors may arise in computing the horizontal pressure-gradient force in terrain-following coordinates, particularly in the presence of steep terrain (cf. Janjic 1977; Mahrer 1984; Dempsey and Davis 1998).

Recently Schär et al. (2002) have proposed a generalization of the traditional terrain transformation in height coordinates (Gal-Chen and Sommerville 1975) that gradually smoothes out small-scale structure in the terrain-following coordinate surfaces with increasing height above the surface. This nonlocal transformation appears to have good potential for reducing the adverse influence of steep and small-scale terrain features in numerical solutions with terrain-following coordinates. In evaluating this nonlocal transformation, Schär et al. conducted nonhydrostatic mountain wave simulations for flow over a mountain profile containing significant small-scale structure. Using the traditional local terrain transform in the Canadian semi-Lagrangian Mesoscale Compressible Community (MC2) model, they encountered significant distortion of the steady mountain-wave structure (cf. their Fig. 15a), which was effectively removed in simulations with their generalized coordinate transform. This distortion can also arise in Eulerian models; using the publicly available version of the Weather Research and Forecasting (WRF) prototype model (available online at wrf-model.org) we found that this distortion would either appear or not appear, depending on the order of accuracy used in computing the advection terms. In further analysis of these results, we have found that for both the semi-Lagrangian and Eulerian codes, the distortion arises when the metric terms in the coordinate transformation are computed using numerics that are not consistent with the numerical schemes used for other terms in the equations, and that the problem can be remedied by suitably altering these numerics.

To understand this behavior, we investigate the nature of truncation errors in simulating flow over terrain at nonhydrostatic scales, and find that these errors may be significant unless the horizontal derivatives are computed in a consistent manner in terrain-following coordinates, such that the portions of mean fields that vary only in z cancel numerically in the finite-difference equations. The metric terms contained in the horizontal derivatives are present in the linear system of equations in terrain-following coordinates and thus may introduce errors even for small-amplitude terrain and weakly sloped coordinate surfaces. Analysis of the linear

* The National Center for Atmospheric Research is sponsored by the National Science Foundation.

Corresponding author address: Dr. Joseph Klemp, NCAR, P.O. Box 3000, Boulder, CO 80307.
E-mail: klemp@ucar.edu

steady-state finite-difference equations for mountain wave flow reveals that inconsistent differencing of the metric terms produces inhomogeneous terms in the linear wave equation. The particular solutions resulting from these terms produce artificial contributions to the wave solution that may be particularly significant for terrain features that have horizontal length scales similar to the Scorer parameter (i.e., $2\pi U/N$).

To document this behavior, we derive the steady-state solution for the linear finite-difference equations in section 2, and present in section 3 examples that illustrate the truncation errors that can arise when the appropriate metric terms do not cancel numerically. In section 4, we show corresponding solutions using a nonlinear nonhydrostatic Eulerian model to verify that the linear analytic results are confirmed in the full numerical model simulations. In section 5, we discuss how the magnitude and appearance of distortions produced by an imbalance in the metric terms depend on the horizontal scale of the terrain. As mentioned above, these truncation errors can also arise in a semi-Lagrangian model; in section 6 we analyze how they occur and discuss how they can be avoided. Summary remarks follow in section 7.

2. Linear analytic mountain-wave solution

The need for consistency in the differencing of the metric terms in terrain-following coordinates can be demonstrated in the context of the linear system of equations. To this end, we will consider solutions to the linear steady-state Boussinesq equations expressed in the Gal-Chen and Sommerville (1975) terrain-following coordinate:

$$\zeta = \frac{z - h}{z_t - h} z_t, \tag{1}$$

where $h(x)$ represents the terrain contour and z_t is the height of the top of the domain.

For this analysis, we will include the capability to reduce the errors in the horizontal pressure-gradient term by removing a reference pressure profile $\pi_{\text{ref}}(z)$ from the total pressure [defined in terms of a normalized Exner function $\pi = c_p\theta_0(p/p_0)^{(R/c_p)}$] before transforming the horizontal derivative to terrain-following coordinates. For this purpose, we define

$$\pi = \pi_{\text{ref}} + \pi_1 + \pi', \tag{2}$$

where $\overline{\pi} = \pi_{\text{ref}}(z) + \pi_1(z)$ represents the actual mean pressure and π' the perturbation from the mean. Ideally, one would like to choose π_{ref} to represent the actual mean pressure such that $\pi_1 = 0$. However, in many applications the mean atmosphere is not a function of z only and may change over time (as in real atmospheric environments). Also, if there is strong variation in the vertical structure of the mean atmosphere, π_{ref} is typically chosen to represent a smoother reference sounding.

In the Boussinesq equations, the pressure-gradient and buoyancy terms in the vertical momentum equation are typically written as (cf. Ogura and Phillips 1962)

$$\frac{\partial(\pi - \pi_0)}{\partial z} - (b - g), \tag{3}$$

where $b = g\theta/\theta_0$ is the buoyancy variable and π_0 is the pressure that is in hydrostatic balance for an atmosphere of constant potential temperature θ_0. To recast (3) in terms of a specified reference state, we represent the buoyancy variable in the same form as the pressure in (2):

$$b = b_{\text{ref}} + b_1 + b', \tag{4}$$

where $\overline{b} = b_{\text{ref}}(z) + b_1(z)$ is the true mean state and b' is the perturbation. In the absence of perturbations, the mean state must be in hydrostatic balance such that

$$\frac{\partial}{\partial z}(\pi_{\text{ref}} + \pi_1 - \pi_0) = b_{\text{ref}} + b_1 - g. \tag{5}$$

By using the definitions (2) and (4) together with (5), it can be readily verified that, to the order of the Boussinesq approximation, the pressure-gradient and buoyancy terms in (3) can be alternatively written as

$$\frac{\partial(\pi - \pi_0)}{\partial z} - (b - g) = \frac{\partial(\pi - \pi_{\text{ref}})}{\partial z} - (b - b_{\text{ref}}) = \frac{\partial \pi'}{\partial z} - b'. \tag{6}$$

Representing the pressure and buoyancy as described above, the 2D inviscid nonhydrostatic Boussinesq equations can be written

$$u\frac{\partial u}{\partial x} + \omega\frac{\partial u}{\partial \zeta} + \frac{\partial(\pi - \pi_{\text{ref}})}{\partial x} + \frac{\partial(\pi - \pi_{\text{ref}})}{\partial \zeta}\zeta_x = 0, \tag{7}$$

$$u\frac{\partial w}{\partial x} + \omega\frac{\partial w}{\partial \zeta} + \frac{\partial(\pi - \pi_{\text{ref}})}{\partial \zeta}\zeta_z - (b - b_{\text{ref}}) = 0, \tag{8}$$

$$u\frac{\partial b}{\partial x} + \omega\frac{\partial b}{\partial \zeta} = 0, \tag{9}$$

$$\frac{\partial u}{\partial x} + \frac{\partial u}{\partial \zeta}\zeta_x + \frac{\partial w}{\partial \zeta}\zeta_z = 0, \quad \text{and} \tag{10}$$

$$\omega \equiv \frac{d\zeta}{dt} = u\zeta_x + w\zeta_z = \zeta_z(w - uz_x). \tag{11}$$

In linearizing these equations about a small terrain height h, the metric terms arising from the terrain-following coordinate transformation become

$$\zeta_z \equiv \frac{\partial \zeta}{\partial z} = \frac{z_t}{z_t - h} \simeq 1 + \frac{h}{z_t} \quad \text{and} \tag{12}$$

$$\zeta_x \equiv \frac{\partial \zeta}{\partial x} = -\frac{z_t - \zeta}{z_t - h}h_x \simeq -\left(1 - \frac{\zeta}{z_t}\right)h_x. \tag{13}$$

Thus, ζ_x and ω are perturbation quantities. In addition,

the buoyancy gradient along constant ζ surfaces may be written

$$\left.\frac{\partial b}{\partial x}\right|_{\zeta} = \left.\frac{\partial}{\partial x}(\bar{b} + b')\right|_{\zeta} = \left.\left[\frac{\partial b'}{\partial x} + N^2 z_x\right]\right|_{\zeta}, \quad (14)$$

where $N^2 = d\bar{b}/dz$, and $z_x|_{\zeta} = -\zeta_x/\zeta_z$. Similarly,

$$\left.\frac{\partial}{\partial x}(\pi - \pi_{\rm ref})\right|_{\zeta} = \left.\frac{\partial}{\partial x}(\pi_1 + \pi')\right|_{\zeta} = \left.\left[\frac{\partial \pi'}{\partial x} + \pi_{1z} z_x\right]\right|_{\zeta}. \quad (15)$$

Thus, the metric term in (15) is present even in linear systems unless the $\pi_{\rm ref}$ chosen is the actual mean pressure.

Retaining only first-order perturbation terms in (7)–(11), the linear equations in terrain-following coordinates for an atmosphere having constant mean wind U and Brunt–Väisälä frequency N become

$$U\frac{\partial u'}{\partial x} + \left[\frac{\partial \pi'}{\partial x} + \pi_{1z} z_x\right] - \pi_{1z} z_x = 0, \quad (16)$$

$$U\frac{\partial w}{\partial x} + \frac{\partial \pi'}{\partial \zeta} - b' = 0, \quad (17)$$

$$U\left[\frac{\partial b'}{\partial x} + N^2 z_x\right] + N^2(-U z_x + w) = 0, \quad \text{and} \quad (18)$$

$$\frac{\partial u'}{\partial x} + \frac{\partial w}{\partial \zeta} = 0. \quad (19)$$

Here, the pressure-gradient and buoyancy terms in (17) have been represented using the second equality in (6).

At this point, the issue of consistency in the numerical treatment of terms in (16)–(19) is readily apparent. In (16), the metric terms $\pm\pi_{1z} z_x$ should cancel such that the linear horizontal momentum equation has the same form as in the Cartesian framework, and, similarly, the $\pm UN^2 z_x$ terms should cancel in (18). However, for this to occur in the numerical model, in (16) the differencing of pressure along constant ζ surfaces (term in brackets) must have the same representation as the differencing of the metric z_x in the last term, and in (18) the differencing of the horizontal advection term (term in brackets) must be the same as the differencing of the metric z_x used in the definition of ω (last term). If this consistency in finite differencing is not enforced, nonhomogeneous terms arise in the linear wave equation that may produce distortions in wave solutions.

To clarify the nature and significance of these numerical distortions, we derive analytic solutions to the finite-difference form of the Eulerian equations (16)–(19). For this purpose, we Fourier transform (16)–(19) in x and represent the horizontal wavenumbers k taking into account the particular finite differencing of each x derivative term in the equations. For example, with second- and fourth-order centered differencing on an unstaggered grid, transforming the finite-difference stencil yields

$$k_2 = \frac{1}{\Delta x}\sin k\Delta x \quad \text{and} \quad (20)$$

$$k_4 = \frac{1}{6\Delta x}(8\sin k\Delta x - \sin 2k\Delta x), \quad (21)$$

respectively. Similarly, on a staggered grid, the second- and fourth-order finite differencing centered at the midpoint between grid points yields

$$k_{2s} = \frac{2}{\Delta x}\sin\frac{1}{2}k\Delta x \quad (22)$$

$$k_{4s} = \frac{1}{12\Delta x}\left(27\sin\frac{1}{2}k\Delta x - \sin\frac{3}{2}k\Delta x\right), \quad (23)$$

respectively. In this manner, the transform of (16)–(19) can be written

$$ik_a U\hat{u} + ik_\pi\hat{\pi} + i(k_\pi - k_\zeta)\pi_{1z}\hat{z} = 0, \quad (24)$$

$$ik_a U\hat{w} + \frac{\partial\hat{\pi}}{\partial\zeta} - \hat{b} = 0, \quad (25)$$

$$ik_a U\hat{b} + N^2\hat{w} + i(k_a - k_\omega)N^2 U\hat{z} = 0, \quad \text{and} \quad (26)$$

$$ik_d\hat{u} + \frac{\partial\hat{w}}{\partial\zeta} = 0, \quad (27)$$

where $\hat{}$ denotes Fourier transformed variables and k_a, k_π, k_ζ, k_ω, and k_d represent the finite-difference approximations for k arising from the various x derivative terms in (16)–(19). For simplicity, in this analysis we assume that the coefficients of the transformed perturbation variables are constants. This requires that U and N are constant as mentioned previously, and that π_{1z} is a constant. This latter assumption is appropriate to the order of the Boussinesq approximation in which the z dependence of the potential temperature multiplying the horizontal pressure gradient is ignored. Combining (24)–(27), we obtain the steady-state wave equation:

$$\frac{\partial^2\hat{w}}{\partial\zeta^2} + \beta^2\hat{w} = P_1 + P_2, \quad (28)$$

where

$$\beta^2 = \frac{k_d k_\pi}{k_a^2}\left(\frac{N^2}{U^2} - k_a^2\right), \quad (29)$$

and P_1 and P_2 are inhomogeneous terms associated with the $\hat{z}$ terms, which are expressed in terms of $\hat{h}$ using the Fourier transforms of the metric expressions (12) and (13):

$$P_1 = -i(k_\pi - k_\zeta)\frac{k_d}{k_a}\frac{\pi_{1z}}{Uz_t}\hat{h} \quad \text{and} \tag{30}$$

$$P_2 = -i(k_a - k_\omega)\frac{k_d k_\pi}{k_a^2}\frac{N^2}{U}\left(1 - \frac{\zeta}{z_t}\right)\hat{h}. \tag{31}$$

Solving (28)–(31) subject to the boundary conditions $\hat{w}(k, 0) = ik_\omega U\hat{h}$ and a radiation condition as $z \to \infty$ yields

$$\hat{w} = -i(K_{P_1} + K_{P_2})U\hat{h} + iK_H U\hat{h}\begin{cases}\exp[i\ \mathrm{sgn}(k)\beta\zeta] & k_a < \dfrac{N}{U} \\ \exp(-\sqrt{-\beta^2}\zeta) & k_a > \dfrac{N}{U},\end{cases} \tag{32}$$

where

$$K_{P_1}(k, \zeta) = \frac{k_a}{k_\pi}\frac{k_\pi - k_\zeta}{N^2 - k_a^2U^2}\frac{\pi_{1z}}{z_t}, \tag{33}$$

$$K_{P_2}(k, \zeta) = \frac{k_a - k_\omega}{N^2 - k_a^2U^2}\left(1 - \frac{\zeta}{z_t}\right)N^2, \quad \text{and} \tag{34}$$

$$K_H(k) = k_\omega + K_{P_1}(k, 0) + K_{P_2}(k, 0). \tag{35}$$

In (32), we are assuming that there are no errors due to finite differencing in the vertical.

Taking the inverse Fourier transform of $\hat{w}(k, \zeta)$ recovers the solution

$$w(x, \zeta) = -\frac{U}{\pi}\int_0^{k^*}\hat{h}K_H \sin(\beta\zeta + kx)\,dk - \frac{U}{\pi}\int_{k^*}^{\pi/\Delta x}\hat{h}K_H \exp(-\sqrt{-\beta^2}\zeta)\sin kx\,dk + \frac{U}{\pi}\int_0^{\pi/\Delta x}\hat{h}(K_{P_1} + K_{P_2})\sin kx\,dk, \tag{36}$$

where k^* is the value of k for which $k_a = N/U$. Notice that the particular solutions [third term in Eq. (36)] corresponding to the spurious inhomogeneous terms P_1 and P_2 contain a singularity in the integrand (in the expressions for K_{P_1} and K_{P_2}) at $k_a = N/U$. Although the integral converges in principal value, this behavior suggests that errors produced by inconsistent differencing of the metric terms will be most noticeable when the terrain forcing has significant amplitude at horizontal wavenumbers in the vicinity of N/U. These particular solutions have a large vertical scale; the amplitude of the K_{P_1} solution is constant with height in this analysis, while the K_{P_2} solution decreases linearly with height across the model domain.

3. Example linear solutions

To illustrate the nature of these finite-difference errors, we consider a terrain profile that Schär et al. (2002) used for testing alternative terrain-following coordinate transformations. This profile is given by

$$h(x) = H\exp\left(-\frac{x^2}{a^2}\right)\cos^2\frac{\pi x}{\lambda} \tag{37}$$

and has the Fourier transform

$$\hat{h}(k) = \frac{\sqrt{\pi}}{4}Ha\left\{2\exp\left(-\frac{1}{4}a^2k^2\right) + \exp\left[-\frac{1}{4}a^2(\kappa - k)^2\right] + \exp\left[-\frac{1}{4}a^2(\kappa + k)^2\right]\right\} \tag{38}$$

with $\kappa = 2\pi/\lambda$, which provides the expression for $\hat{h}(k)$ used in the numerical evaluation of (36). Following Schär et al., we define $H = 250$ m, $\lambda = 4000$ m, and $a = 5000$ m, and specify a constant mean state with $N = 0.01\ \mathrm{s}^{-1}$ and $U = 10\ \mathrm{m\ s}^{-1}$. For the terrain transformation (1), we set $z_t = 21$ km for consistency with the numerical simulations that will be presented in section 4. Solutions will be considered for $\Delta x = 500$ m, implying a primary ridge spacing of $8\Delta x$. For these conditions, $2\pi U/N = 6.28$ km, which is about 50% larger than the major ridge spacing in (37). Thus, these conditions should be favorable, though not optimal, for exciting the spurious inhomogeneous portion of the solution in (36).

In evaluating the influence of the horizontal finite differencing on the steady linear wave solution, we assume the variables are situated on a C grid such that the horizontal velocity is staggered in x at the midpoint between the location of the other variables. We initially assume that $h(x)$ is defined in the same x location as w, b, and π, although we shall later consider the effect of shifting h to the location of u. For simplicity, we will examine only the effects of second- and fourth-order horizontal differencing, which will be either staggered or unstaggered depending on the position of the differenced variable relative to the location of the term being evaluated. Thus, each of the finite-difference approximations to k in the solution given by (33)–(36) will be represented by k_2, k_4, k_{2s}, or k_{4s} as defined in (20)–(23).

The vertical velocity field displayed in Fig. 1a is computed with fourth-order differencing for the advection terms ($k_a = k_4$) and the metric used to compute ω ($k_\omega = k_4$), together with second-order staggered differencing for the horizontal pressure gradient ($k_\pi = k_{2s}$), the metric multiplying the mean vertical pressure gradient ($k_\zeta = k_{2s}$), and the horizontal velocity gradient in the divergence equation ($k_d = k_{2s}$). In this case, the metric terms contributing to the artificial inhomogeneous solution in (36) vanish identically ($K_{P1} = K_{P2} = 0$), and the displayed field is indistinguishable from the exact solution obtained by using k instead of the various finite-difference approximations to k in (33)–(36).

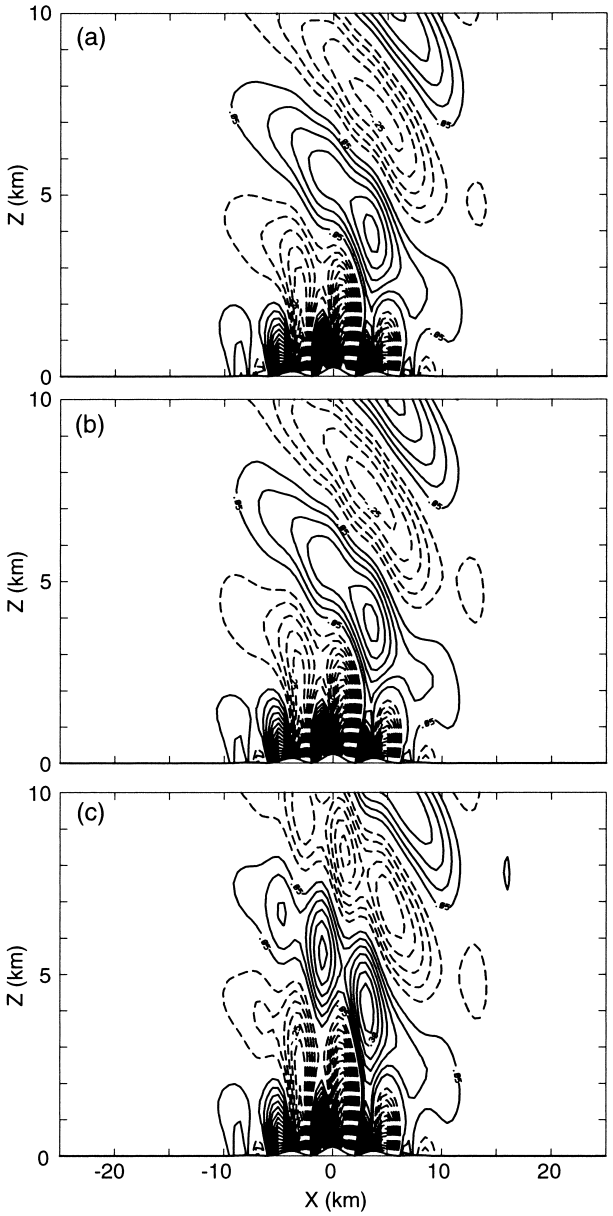

FIG. 1. Vertical velocity from the analytic solution for the linear finite-difference equations with $k_\pi = k_\zeta = k_d = k_{2s}$, and (a) $k_a = k_\omega = k_4$, (b) $k_a = k_\omega = k_2$, and (c) $k_a = k_4$, $k_\omega = k_2$. Contour interval is 0.05 m s^{-1}.

A point of clarification is in order regarding the display of these linear solutions. The fields shown in Fig. 1 represent the linear solution for $w(x, \zeta)$ for flow over terrain of height H. The plotted fields have been transformed from the (x, ζ) coordinate to (x, z) such that w satisfies the correct lower boundary condition at the terrain surface $z = h$. They differ slightly in appearance from the fields one would obtain if $w(x, \zeta)$ were plotted assuming $\zeta \simeq z$, in which case the lower boundary condition is satisfied at $z = 0$. Both solutions are equivalent to first order. However, satisfying the lower boundary

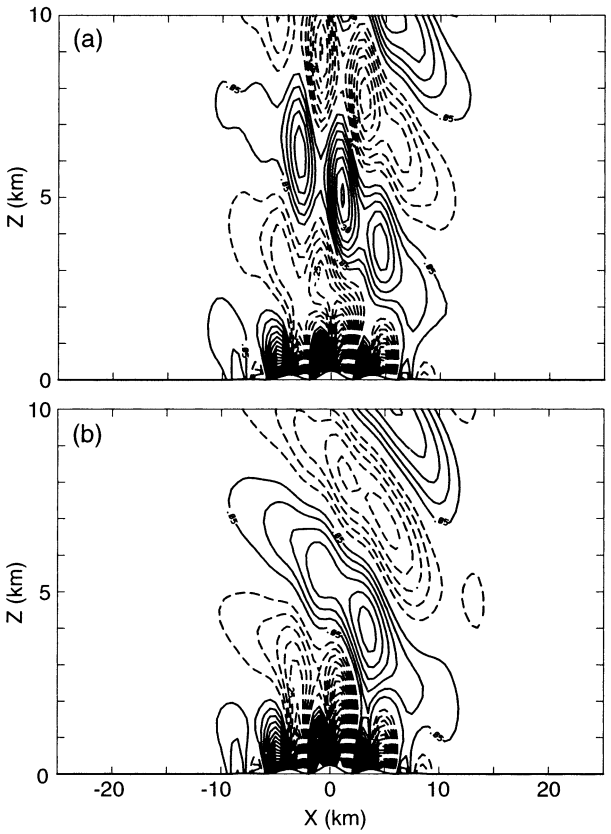

FIG. 2. As in Fig. 1a except $k_\pi = k_{4s}$, and (a) $\pi_{1z} = -g$ and (b) $\pi_{1z} = -0.1g$.

condition at $z = h$ leads to exact nonlinear solutions to the linear Long's equation, and is also consistent with the way fields are displayed in the full simulation model discussed in the next section.

The vertical velocity shown in Fig. 1b is obtained in the same manner as the solution in Fig. 1a except that all x derivatives are computed with second-order differencing ($k_a = k_\omega = k_2$, $k_\pi = k_\zeta = k_{2s}$). The artificial metric terms again cancel identically and the solution differs only slightly from that in Fig. 1a. Now suppose we recompute the solution for the same conditions as in Fig. 1b except we use fourth-order differencing for the advection terms ($k_a = k_4$). Instead of improving the solution, there is a significant distortion of the vertically propagating wave aloft (Fig. 1c). This distortion is caused by the differing numerical treatment of the metric terms ($\pm N^2 U z_x$) in (18) that excites the inhomogeneous solution represented by K_{P2}.

To examine the influence of the metric terms associated with the horizontal pressure gradient in (16), we examine the linear solution obtained with the same differencing as used for Fig. 1a, except we increase the numerical accuracy of the horizontal pressure gradient term to fourth order ($k_\pi = k_{4s}$). In this case, the $\pm \pi_{1z} z_x$ terms in (16) do not cancel numerically and the inhomogeneous solution represented by K_{P1} can distort the

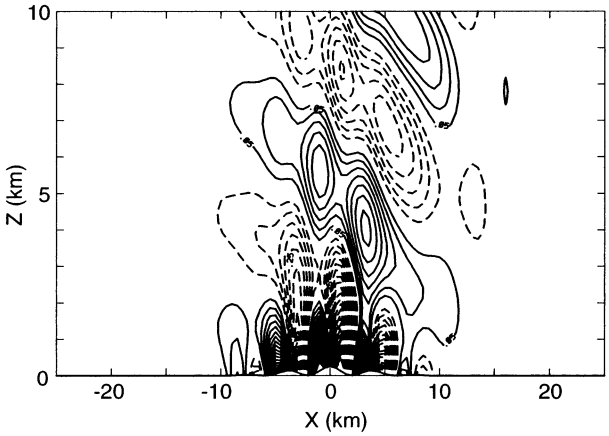

FIG. 3. As in Fig. 1c except $k_\omega = k_{2s}$ and $k_\zeta = k_2$.

solution. The significance of this imbalance depends on the magnitude of the mean vertical pressure gradient π_{1z} that remains after a reference pressure profile π_{ref} has been removed from the pressure field. To illustrate the effect of subtracting a reference pressure profile from the full pressure, we display first in Fig. 2a the solution that results when no reference pressure is utilized ($\pi_{\text{ref}} = 0$), which exhibits significant distortion of the flow. On the other hand, choosing a reference pressure that equals the actual mean pressure would eliminate π_{1z} and the solution in Fig. 2a would become identical to that in Fig. 1a. As mentioned above, in practice it is usually not possible to remove all of the mean pressure with a reference profile. Figure 2b shows the solution arising when 90% of the mean pressure has been removed by the reference profile. This field exhibits only weak distortion due to the imbalance in differencing the metric terms associated with the horizontal pressure gradient. The imbalance is partly mitigated by the fact that the second- and fourth-order differencing of the metric terms are computed on a staggered grid, which increases the accuracy over unstaggered differencing (cf. Durran 1999, p. 115). However, either decreasing the resolution or increasing the magnitude of π_{1z} will further increase these errors.

In the examples discussed above, the differencing was based on the terrain height being defined in the same horizontal location as the thermodynamic variables. If instead, h is collocated horizontally with the horizontal velocity, consistent differencing of the metric terms in (16) and (18) will not be possible under any circumstances. In (16), k_π and k_ζ will be differenced on staggered and unstaggered grids, respectively, and a similar situation arises in (18) for k_ω and k_a. Figure 3 displays the solution for fourth-order advection, comparable to Fig. 1c, except that the staggering of the metric terms k_ω and k_ζ are now reversed such that $k_\omega = k_{2s}$ and $k_\zeta = k_2$. In this solution, 90% of the mean pressure is removed by the reference pressure as in Fig. 2b. In Fig. 3 virtually all of the distortion is caused by the metric imbalance in the pressure terms in (16), which is larger than in Fig. 2b due to the decreased accuracy in differencing $k_\zeta = k_2$.

4. Nonlinear numerical model simulations

We confirm the results obtained from the linear analytic model by simulating mountain wave development under similar conditions using a 2D time-dependent nonlinear nonhydrostatic numerical model. For this purpose, we use an early version of the WRF prototype model in terrain-following height coordinates (Klemp et al. 2000, unpublished manuscript; available online at www.mmm.ucar.edu/individual/skamarock/wrf_equations_eulerian.pdf). This Eulerian solver uses a leapfrog time-splitting technique for integrating the compressible nonhydrostatic equations on a C grid. The terrain height h is defined beneath columns containing the thermodynamic variables, and horizontal differences can be specified using either second- or fourth-order differences. The domain is 50 km $\times$ 21 km with horizontal and vertical grid spacings of 500 and 300 m, respectively. The domain top is set at $z_t = 21$ km, with an absorbing layer in the upper half of the domain to minimize reflection of upward-propagating gravity waves, and open boundary conditions are specified at the lateral boundaries. Terrain-following coordinates are employed as defined by (1), and the terrain height is specified according to (37). The atmosphere is characterized by the same constant mean wind $U = 10$ m s^{-1} and stability $N = 0.01$ s^{-1} as in the linear solutions in the previous section.

The vertical velocity fields for the same combinations of second- and fourth-order differencing used in Fig. 1 are displayed in Fig. 4 for the model simulations at $t = 5$ h, when the fields are essentially at steady state. With fourth-order differencing for advection and the horizontal metric term in ω together with second-order staggered differencing for both pieces of the horizontal pressure gradient term, the appropriate metric terms cancel numerically and the solution (Fig. 4a) is similar to the linear analytic solution. The primary difference between the vertical velocity in Fig. 4a and Fig. 1a arises because the numerical model describes the compressible atmosphere in which the wave amplitudes increase with height in proportion to the inverse square root of density, while in the Boussinesq analytic solution the wave amplitude is constant with height. The model solution using second-order differencing for horizontal advection (Fig. 4b) together with second-order calculation of the horizontal metric term in ω produces nearly the same result as expected, since the metric terms are treated consistently. However, with fourth-order horizontal advection and a second-order horizontal metric term in ω (Fig. 4c), the same distortion arises as in Fig. 1c due to noncancellation of metric terms in the buoyancy equation.

In these simulations, the reference pressure removed from the pressure gradient terms corresponds to a constant potential temperature atmosphere. Thus, the perturbation pressure includes a portion of the pressure

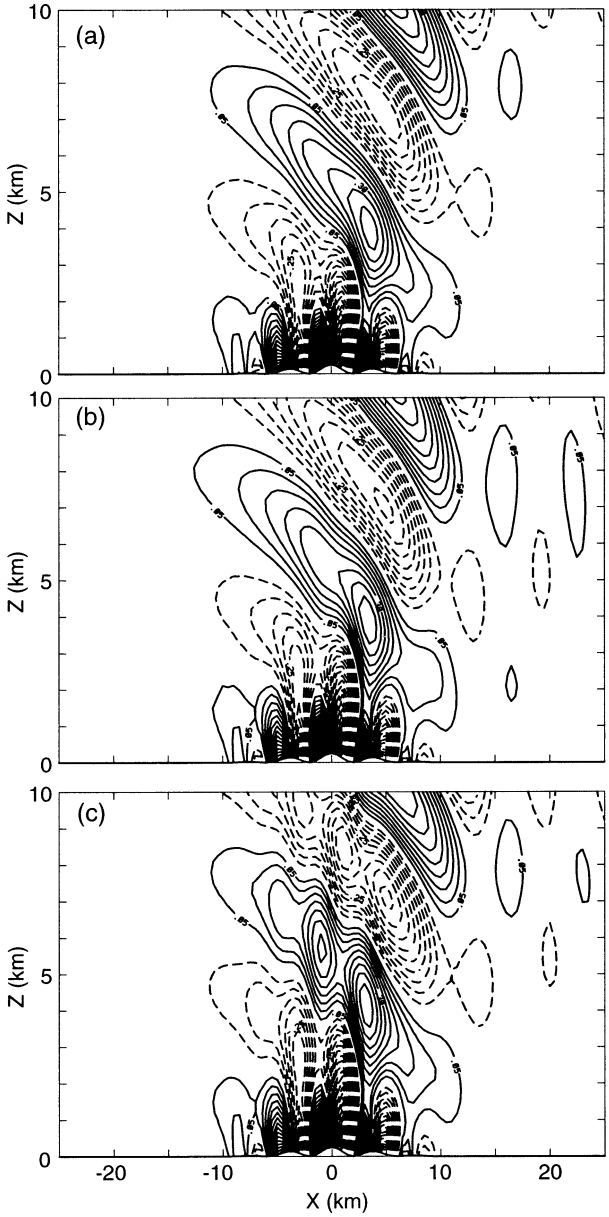

FIG. 4. Numerical simulation of vertical velocity with horizontal finite differencing as in Fig. 1.

corresponding to the difference between the actual mean pressure and the reference pressure for a neutral atmosphere. Repeating the simulation shown in Fig. 4a but increasing the accuracy of the horizontal pressure gradient term to a fourth-order staggered difference [as in (23)], the solution (Fig. 5) is actually degraded somewhat since the metric terms associated with the horizontal pressure gradient no longer cancel (similar to Fig. 2b). Again, with coarser resolution or greater deviation of the reference pressure from the full pressure, this distortion will increase.

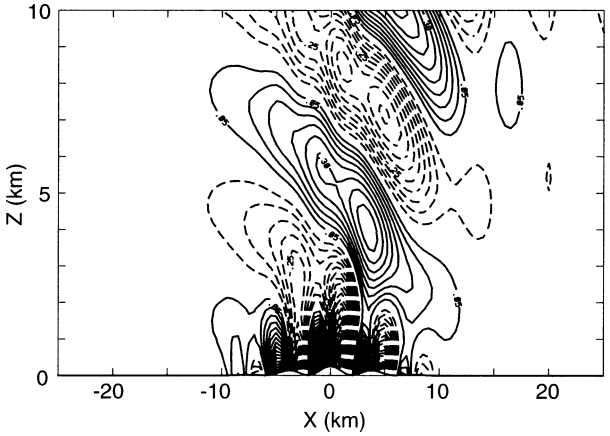

FIG. 5. As in Fig. 4a except $k_{\pi} = k_{4s}$.

5. Dependence on horizontal scale

As mentioned previously, inconsistent differencing of metric terms appears to have its most pronounced influence at horizontal scales in the vicinity of N/U, where the artificial particular solutions (32)–(34) to the inhomogeneous wave equation (28) become singular. To illustrate this dependence, we consider linear analytic solutions for the same terrain profile (37), but for different horizontal length scales.

Recall that for the solutions shown in Fig. 1, the major ridge spacing is about 4 km, which is somewhat smaller than the length scale (6.28 km) at which $k = N/U$. Thus, waves at the scale of the ridge spacing are evanescent and the longer wavelength vertically propagating modes aloft exhibit a structure that is nearly hydrostatic in appearance. Figure 6a displays the exact linear analytic solution for vertical velocity for the case with twice the horizontal scale in the terrain profile ($\lambda = 8$ km, $a = 10$ km) as shown in Fig. 1. (The small irregularities in the displayed contours are due to calculation of this solution on the same grid as used in the numerical simulations.) In this situation, waves at the scale of the primary ridge spacing are slightly longer than the evanescent cutoff and can propagate vertically. The solution has the characteristic appearance of vertically propagating nonhydrostatic waves extending above and downstream of the ridges. With fourth-order finite differencing for advection ($k_a = k_4$) and second-order evaluation of the metric term in ω ($k_{\omega} = k_2$) with $\Delta x = 1$ km, significant numerical truncation errors are apparent in the steady-state vertical velocity field (Fig. 6b). This is the same finite differencing as used in the case shown in Fig. 1c. The scale of the artificial inhomogeneous solution is similar to that of the vertically propagating mode, which gives a stronger distortion than in Fig. 1c and with a differing overall appearance.

Increasing the width of the terrain substantially, the mountain wave structure becomes essentially hydrostatic. At these scales, the dominant wavenumbers in the artificial inhomogeneous portion of the solution in

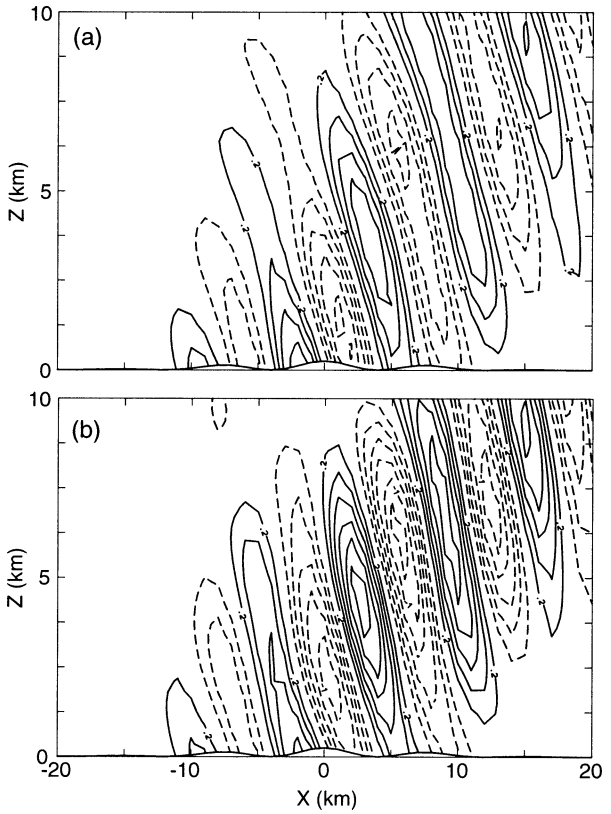

FIG. 6. Vertical velocity from the linear analytic solution for the case shown in Fig. 1 except with twice the horizontal length scale in the terrain profile ($\lambda = 8$ km, $a = 10$ km). (a) Solution with exact numerics; (b) solution with the same horizontal finite differencing as in Fig. 1c. Contour interval is 0.2 m s^{-1}.

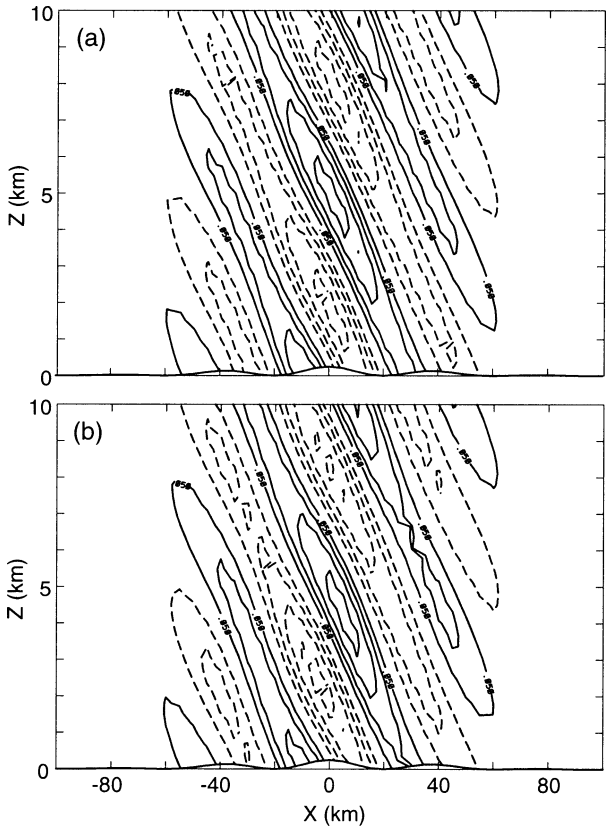

FIG. 7. As in Fig. 6 except with 10 times the horizontal length scale in the terrain profile as in Fig. 1 ($\lambda = 40$ km, $a = 50$ km). Contour interval is 0.05 m s^{-1}.

(32) are far from the singularity at $k = N/U$. Figure 7a shows the linear analytic vertical velocity over terrain defined by (37) with $\lambda = 40$ km and $a = 50$ km. For comparison, the vertical velocity computed on a 5-km horizontal grid with the same finite differencing as used for Fig. 6b is shown in Fig. 7b. Although the inconsistent numerical treatment of the metric terms in (18) contributes to an artificial component to the wave solution, the amplitude of this distortion is small.

6. Consistent metrics in a semi-Lagrangian model

In the preceding analytic analysis and model simulations, we have focused on the treatment of the metric terms associated with the terrain-following coordinate transformation in an Eulerian finite-difference model. However, as mentioned in the introduction, truncation errors having the character of those evident in Fig. 1c were originally encountered in the Canadian MC2 semi-Lagrangian model (Schär et al. 2002). This result is displayed in Fig. 8 for the same model configuration as described in section 4 for the Eulerian model. This C-grid model uses a second-order finite difference over one grid interval for both the horizontal pressure difference and the metric adjustment to that pressure difference, which provides a consistent treatment of the horizontal pressure gradient terms. Advection is accommodated using a semi-Lagrangian time step, with a third-order interpolation of variables to the departure

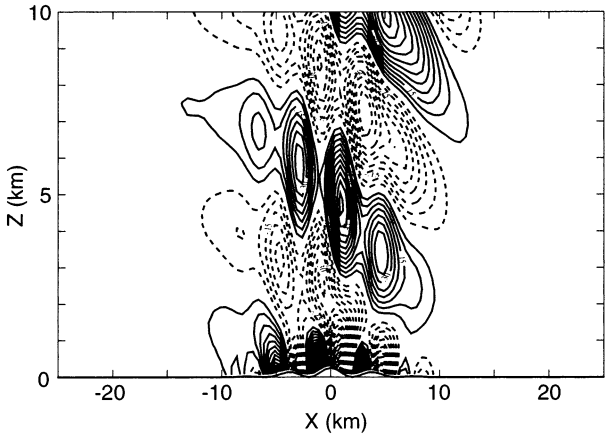

FIG. 8. Numerical simulation of vertical velocity using the semi-Lagrangian MC2 model for comparison with Eulerian analytic (Fig. 1) and numerical (Fig. 4) solutions. Contour interval is 0.05 m s^{-1}. [After Schär et al. (2002).]

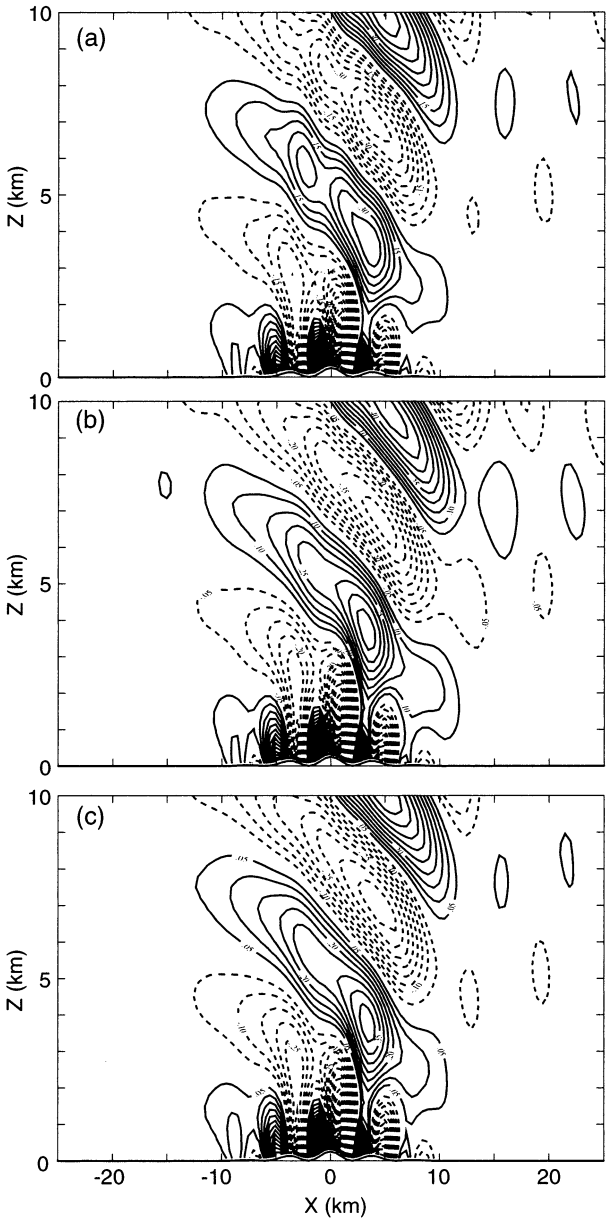

FIG. 9. As in Fig. 8 except with second-order interpolation to the semi-Lagrangian departure points in (a) computational space using (u, ω) with an 8-s time step, (b) computational space using (u, ω) with a 1-s time step, and (c) physical space using (u, w) with an 8-s time step.

point that is calculated in computational space [i.e., using (u, ω) to locate the departure point, and interpolating variables to the departure point in the (x, ζ) coordinate]. The relationship between ω and w [Eq. (11)] uses a second-order difference over $2\Delta x$ for the ζ_x metric.

It appears that the third-order semi-Lagrangian interpolation together with the second-order metric in the ω equation is responsible for the distortion of the steady mountain wave solution evident in Fig. 8. However, these errors cannot be removed by simply matching the order of the semi-Lagrangian interpolation to the order of the metric in the ω equation. This is illustrated in Fig. 9a, where the interpolation has been changed to second order. Although the error has been reduced, it is still significant.

To explain the nature of the metric imbalance for this situation, we return to the linear analysis of Eqs. (7)–(11) and derive the numerical form of the steady-state linear buoyancy equation (9) using second-order interpolation for the semi-Lagrangian advection. Letting (i, k) denote the horizontal and vertical grid indices of the arrival point for the semi-Lagrangian trajectory, the vertical portion of the interpolation becomes

$$b_n^* = b_{n,k} - \lambda_\zeta \left.\frac{\partial b}{\partial \zeta}\right|_n + \frac{1}{2}\lambda_\zeta^2 \left.\frac{\partial^2 b}{\partial \zeta^2}\right|_n$$
$$= b'_{n,k} + N^2(z_{n,k} - \lambda_\zeta). \tag{39}$$

Here, $\lambda_\zeta = \omega_{i,k}\Delta t$ and n represents the particular column in which the interpolation is required (i.e., i, $i+1$, $i-1$). Recall that $b = \overline{b} + b' = N^2 z + b'$, and we assume N is constant with height.

The second-order horizontal interpolation of buoyancy to the departure point (b_d) is similarly given by

$$b_d = b_i^* - \lambda_x \frac{\partial b^*}{\partial x} + \frac{1}{2}\lambda_x^2 \frac{\partial^2 b^*}{\partial x^2}, \tag{40}$$

where $\lambda_x = U\Delta t$. For steady-state flow,

$$\frac{db}{dt} = \frac{b_{i,k}^{t+\Delta t} - b_d^t}{\Delta t} = \frac{b_{i,k}^t - b_d^t}{\Delta t} = 0. \tag{41}$$

Using (39) and (40), Eq. (41) becomes

$$U\frac{\partial b'}{\partial x} + UN^2 z_x + N^2\omega - \frac{1}{2}U^2\Delta t \frac{\partial^2 b'}{\partial x^2}$$
$$- \frac{1}{2}U^2N^2\Delta t z_{xx} = 0, \tag{42}$$

where the x derivatives are evaluated with second-order finite differences. Notice that in addition to the terms in (18), Eq. (42) contains $O(\Delta t)$ terms for the horizontal diffusion of b' plus an additional z_{xx} metric. Although a second-order z_x metric in the omega equation (11) will cancel with the second term in (42), the last term in (42) will contribute an inhomogeneous term to the steady linear wave equation that artificially distorts the solution. Since this is an $O(\Delta t)$ term, decreasing the time step will diminish its influence. This is demonstrated in Fig. 9b, in which the second-order semi-Lagrangian interpolation provides a good solution with the time step reduced to 1 s.

Conducting the interpolation in physical space produces important changes with respect to the appearance of metric terms in the advection terms. We illustrate these differences again with a second-order interpolation, applied first in the vertical:

$$b_n^* = b_{n,k} - (z_{n,k} - z_{i,k} + \lambda_z)\left.\frac{\partial b}{\partial z}\right|_n + \frac{1}{2}(z_{n,k} - z_{i,k} - \lambda_z)^2\left.\frac{\partial^2 b}{\partial z^2}\right|_n = b'_{n,k} + N^2(z_{i,k} - \lambda_z), \quad (43)$$

where $\lambda_z = w_{i,k}\Delta t$. Using (43) in (40), the buoyancy at the departure point is given by

$$b_d = b_{i,k} - \lambda_z N^2 - \lambda_x\frac{\partial b'}{\partial x} + \frac{1}{2}\lambda_x^2\frac{\partial^2 b'}{\partial x^2} \quad (44)$$

and upon substitution into (41) yields

$$U\frac{\partial b'}{\partial x} + N^2 w - \frac{1}{2}U^2\Delta t\frac{\partial^2 b'}{\partial x^2} = 0. \quad (45)$$

By interpolating using (u, w) in physical (x, z) space, no metric terms appear in (45) and the cancellation of metric terms is no longer an issue. Also, since ω does not appear in (45), it no longer matters if the order of the semi-Lagrangian interpolation differs from that used in computing the metric term in the ω equation. Figure 9c illustrates how the the artificial distortion disappears in the MC2 simulation with a second-order interpolation computed in physical space.

The MC2 model actually solves a prognostic equation for the perturbation of temperature from a constant reference temperature. Analysis of the semi-Lagrangian interpolation for the linear temperature equation leads to a similar behavior of the metric terms as discussed above for the buoyancy equation. One difference is that the stability N^2 is replaced by the mean temperature gradient $gd\overline{T}/dz$. Thus, if the mean temperature for the atmosphere is isothermal, the metric terms [similar to the $N^2 z_x$ terms in Eq. (42)] will vanish in the linear temperature equation. Thus, MC2 exhibits no distortion in this test problem when the mean atmosphere is isothermal (confirmed in simulations not shown). However, for nonisothermal conditions (such as our test problem with $N = 0.01\ \mathrm{s}^{-1}$), the perturbation temperature will contain a portion of the mean state and will produce all of the same terms as in (42). An analogous situation arises in semi-Lagrangian models that express the Lagrangian integration of the thermodynamic equation in terms of a perturbation from a specified reference state [i.e., using the notation of (4), db/dt is integrated in the form $d(b_1 + b')/dt + \mathbf{V}\cdot\nabla b_{\mathrm{ref}}$]. For these formulations, the consistency in the semi-Lagrangian trajectory calculation remains an issue to the extent that the specified reference state b_{ref} differs from the actual mean state $\overline{b}$. Furthermore, if $\mathbf{V}\cdot\nabla b_{\mathrm{ref}}$ is evaluated in computational space, the consistency requirements for the numerics used in these terms will be the same as for the Eulerian system.

We have recently become aware of an alternative modification to the semi-Lagrangian procedures in MC2 that appears to remove the truncation errors evident in Fig. 8 (Benoit et al. 2002, unpublished manuscript; available online at www.cmc.ec.gc.ca/rpn/modcom/publi_conf/Poster_211_orography/p211_final.pdf). In evaluating ω from (11), Benoit et al. proposed computing the ''horizontal'' advection of z in a semi-Lagrangian fashion, representing $z_x|_\zeta$ as the difference in height between the arrival and departure points of the trajectory, computed along a constant ζ surface. In the context of our linear analysis, and using the notation from (39) and (40),

$$z_n^* = z_{n,k} - \lambda_\zeta \quad \text{and} \quad (46)$$

$$z_d = z_i^* - \lambda_x z_x^* + \frac{1}{2}\lambda_x^2 z_{xx}^* \quad (47)$$

and the linear form of (11), $\omega = w - Uz_x|_\zeta$, becomes

$$\omega_{i,k} = w_{i,k} - U\frac{z_i^* - z_d}{\lambda_x} = w_{i,k} - Uz_x + \frac{1}{2}U^2\Delta t z_{xx}. \quad (48)$$

Using (48) to represent ω in the third term of (42), Eq. (42) now is equivalent to (45), in which the spurious z_{xx} metric term is not present.

7. Summary

Using both linear analytic and numerical model solutions, we have demonstrated that significant truncation errors may arise in nonhydrostatic simulations in terrain-following coordinates if the metric terms are not treated in a consistent manner. This consistency requires that the influence of mean fields (functions of z only) differenced along sloping coordinate surfaces cancel numerically from the finite-difference equations. If these metric terms are not numerically balanced, spurious contributions to the gravity wave dynamics arise that may significantly distort the evolving flow. This distortion increases in magnitude as the horizontal resolution of significant scales forced by the terrain decreases. These artificial components of the numerical solution are proportional to the terrain height and, thus, remain present even in linear applications where the terrain height and slope are small.

In evaluating the linear analytic finite-difference solutions, it is apparent that the spurious effects of numerical imbalance in the metric terms are most dramatic when the terrain has significant forcing at scales near the wavenumber N/U, where inhomogeneous terms in the linear wave equation (32)–(35) become singular. At hydrostatic scales, although the inhomogeneous terms (33)–(34) may still be present, their influence is substantially reduced (Fig. 7).

This analysis suggests that the terrain height should be defined beneath columns in which the thermodynamic variable and w are defined. This allows consistent differencing of the metric term in ω with whatever order numerics are used in the advection of scalar variables, and consistent treatment of the metric in the horizontal pressure gradient formulation. A consistency issue will

arise, however, in computing the advection term for the horizontal velocity in cases where there is strong mean shear. We have found this potential imbalance to be of significantly less importance than those arising in the scalar advection and pressure gradient terms. Epifanio and Durran (2001) have defined the terrain height on a grid having double the horizontal resolution of the nominal grid such that horizontal metric terms can be computed over a single nominal grid interval for terms evaluated at either thermodynamic or horizontal velocity grid points. This reduces the effect of metric term imbalance by increasing the accuracy of the numerics for the metric terms. However, artificial effects may still arise if the resolution becomes sufficiently coarse.

The consistent differencing of the metric terms in computing horizontal gradients is somewhat different from the traditional issue of errors in horizontal pressure gradient terms in regions of steeply sloped coordinate surfaces. The latter problem is related to difficulties in evaluating the vertical pressure gradient to accurately adjust the pressure gradient along the coordinate surface to one taken at constant height. This problem is accentuated when there is strong curvature in the vertical pressure profile, as occurs in the vicinity of sharp changes in stability. These errors associated with steeply sloped coordinate surfaces may be significant at all scales of motion, including fully hydrostatic scales. The issue of consistent treatment of metric terms that we have addressed here appears to be most significant for the buoyancy advection (through its influence on gravity waves), and may arise even with perfect resolution of the vertical gradients. Its regime of concern includes small terrain slopes, but appears to be restricted to nonhydrostatic scales near $k = N/U$ when these scales are not numerically well resolved.

An alternative approach for achieving accurate representation of horizontal derivatives in terrain-following coordinates is to avoid using the metrics by computing the derivatives in physical space (Mahrer 1984; Dempsey and Davis 1998). The horizontal derivative at grid point (i, k) is then calculated in a two-step process in which 1) the variable is interpolated vertically in columns on either side of column i to the same height as the point (i, k) and then 2) the interpolated values are finite differenced to form the horizontal derivative at constant height. With this approach, the metrics are not used in computing the horizontal derivative, and higher-order interpolation can be used to more accurately represent vertical variation of the mean field. This latter aspect is of primary concern in the traditional problem of computing the horizontal pressure gradient in terrain-following coordinates at hydrostatic scales. However, this two-step technique may require significantly increased computations or array storage (particularly for higher-order horizontal finite differences), and would compromise the conservation properties achieved in finite-volume approaches (particularly for the advection terms).

For semi-Lagrangian models, the consistent evaluation of metric terms is dependent upon the manner in which the interpolation of variables to the departure point is carried out. By interpolating based on (u, ω) in the transformed vertical coordinate, spurious metric terms (that should cancel in the linear system) may arise. These terms cannot be completely removed unless ω is also computed through a Lagrangian integration of (11) (as recently proposed by the MC2 developers). However, by conducting the interpolation using (u, w) in physical space, these metric terms do not arise and thus their consistency in computing advective processes is not an issue. Removing a reference profile from the Lagrangian integration of the thermodynamic variable may reduce the distortion caused by metric inconsistency in the trajectory calculation if the reference profile is close to the actual mean state; however, in many nonlinear or real weather applications, deviations from any specified reference state will be significant.

Acknowledgments. The authors would like to thank Christoph Schär, Dale Durran, and Jim Doyle for their helpful suggestions and for their efforts in conducting confirmatory simulations with other models.

REFERENCES

Dempsey, D., and C. Davis, 1998: Error analysis and tests of pressure-gradient force schemes in a nonhydrostatic, mesoscale model. Preprints, *12th Conf. on Numerical Weather Prediction,* Phoenix, AZ, Amer. Meteor. Soc., 236–239.

Durran, D. R., 1999: *Numerical Methods for Wave Equations in Geophysical Fluid Dynamics.* Springer Press, 465 pp.

Epifanio, C. C., and D. R. Durran, 2001: Three-dimensional effects in high-drag-state flows over long ridges. *J. Atmos. Sci.,* **58,** 1051–1065.

Gal-Chen, T., and R. C. J. Sommerville, 1975: Numerical solutions of the Navier–Stokes equations with topography. *J. Comput. Phys.,* **17,** 276–310.

Janjic, Z. I., 1977: Pressure gradient force and advection scheme used for forecasting with steep and small scale topography. *Beitr. Phys. Atmos.,* **50,** 186–189.

Mahrer, Y., 1984: An improved numerical approximation of the horizontal gradients in a terrain-following coordinate system. *Mon. Wea. Rev.,* **112,** 918–922.

Ogura, Y., and N. W. Phillips, 1962: Scale analysis of deep and shallow convection in the atmosphere. *J. Atmos. Sci.,* **19,** 173–179.

Phillips, N. A., 1957: A coordinate system having some special advantages for numerical forecasting. *J. Meteor.,* **14,** 184–185.

Schär, C., D. Leuenberger, O. Fuhrer, D. Lüthi, and C. Girard, 2002: A new terrain-following vertical coordinate formulation for atmospheric prediction models. *Mon. Wea. Rev.,* **130,** 2459–2480.